New Techniques in the Search for Z' Bosons and Other Neutral Resonances

Christopher Hays
University of Oxford,
Oxford, OX1 3RH, United Kingdom
hays@physics.ox.ac.uk

Ashutosh Kotwal
Duke University,
Durham, NC 27708, USA
kotwal@phy.duke.edu

Oliver Stelzer-Chilton
TRIUMF,
Vancouver, British Columbia V6T 2A3, Canada
stelzer-chilton@triumf.ca

The search for neutral resonances at the energy frontier has a long and illustrious history, resulting in multiple discoveries. The canonical search scans the reconstructed invariant mass distribution of identified fermion pairs. Two recent analyses from the CDF experiment at the Fermilab Tevatron have applied novel methods to resonance searches. One analysis uses simulated templates to fit the inverse mass distribution of muon pairs, a quantity with approximately constant resolution for momenta measured with a tracking detector. The other analysis measures the angular distribution of electron pairs as a function of dielectron mass, gaining sensitivity over a probe of the mass spectrum alone. After reviewing several models that predict new neutral resonances, we discuss these CDF analyses and potential future applications.

I. INTRODUCTION

Searches for neutral resonances have historically brought major breakthroughs by either confirming important predictions or discovering unexpected particles. The 1974 discovery of the J/ψ meson [1] as a $c\bar{c}$ bound state confirmed the GIM mechanism [2] for preventing flavor-changing neutral currents, and the discovery of the Z boson [3] confirmed the gauge unification of the electromagnetic and weak forces [4]. Meanwhile, the discovery of the upsilon [5] was completely unexpected, and increased the number of known fermion generations to three.

Turning to the future, there are reasons to expect the next important particle physics discovery will be a neutral resonance. In addition to the well-motivated Higgs boson [6] of the standard model (SM), there are many new resonances predicted by proposed extensions to the standard model. These extended theories can address unexplained features of the SM, such as: the lack of gauge unification and the hierarchy between the electroweak and Planck scales (through supersymmetry [7] or the presence of extra dimensions [8]); and parity violation and light neutrino masses (through an additional $SU(2)_R$ gauge symmetry [9], which has weak couplings to right-handed fermions).

The most sensitive direct searches for neutral resonances at high mass come from Tevatron $p\bar{p}$ collision data. Future searches in pp collisions from the Large Hadron Collider (LHC) [10] will increase the probed mass range. As larger datasets with higher energies are studied, enhancements to the search strategy can improve sensitivity and facilitate the analysis. Such enhancements have been developed and applied to searches for new resonances in the CDF dimuon [11] and dielectron [12] data.

II. MODELS CONTAINING NEUTRAL RESONANCES

A neutral resonance decaying to fermion pairs can have intrinsic spin equal to 0, 1, or 2. No fundamental scalar particle has yet been observed, though the SM requires one in the form of a Higgs boson. Beyond the SM, there could be multiple Higgs bosons with varying properties [13]. In supersymmetric models, there are spin-0 partners to fermions that could be produced as resonances in $p\bar{p}$ or pp collisions [14]. Any model with an additional U(1) gauge group will have a new spin-1 gauge boson, generically referred to as a Z' boson [15, 16]. Models of extra dimensions at the electroweak scale predict spin-2 graviton resonances [17, 18].

A. Sneutrino Production in Hadron Collisions

To remove the fine-tuning of the Higgs boson mass, the scale of supersymmetry should be of the same order as the electroweak scale, making the discovery of supersymmetry likely at the Tevatron or LHC (should it exist). The supersymmetric partner to the neutrino has no electromagnetic charge and is thus a candidate for production as a neutral resonance.

Resonant sneutrino production would violate R-parity, a multiplicative quantum number that is $+1$ for matter and -1 for supersymmetric matter. The violation of R-parity implies that the lightest sparticle is not stable, potentially removing it as a candidate for dark matter. However, if the lightest sparticle has sufficiently small couplings to give it a lifetime on the order of the age of the universe, it can still be a dark-matter candidate [19].

Proton decay limits require at least one set of R-parity-violating terms to be vanishingly small [20]. This can be accomplished by imposing a "baryon parity" that conserves baryon number and suppresses proton decay more than R-parity conservation [21]. With baryon parity there are two sets of R-parity-violating Yukawa terms in the Lagrangian, both of which are consistent with proton decay limits and relevant for sneutrino production and decay at a hadron collider:

$$\mathcal{L}_{\not{R}} = \lambda_{ijk} L_i L_j e_k^c + \lambda'_{ijk} L_i Q_j d_k^c, \tag{1}$$

where Q (d) and L (e) are SU(2)$_L$ doublet (singlet) superfields. As shown in Fig. 1, the first term governs sneutrino decay to leptons and the second term governs sneutrino production in hadron collisions. Because of the d_k^c superfield in the production term, only-down type quark interactions produce sneutrinos, with λ'_{i11} the most relevant coupling at the Tevatron and LHC (due to parton distributions in the proton).
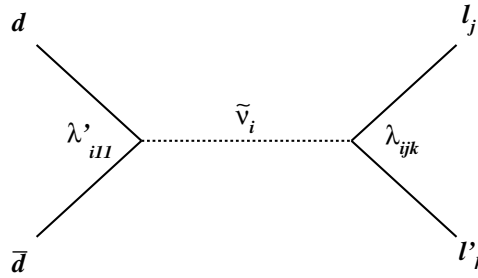

FIG. 1: The Feynman diagram for resonant sneutrino production at a hadron collider.

The total width of a new resonance is an important parameter in a search, in particular relative to the detector mass resolution. The partial width of a given sneutrino decay is [22, 23]:

$$\Gamma(\tilde{\nu}_i \to f_j f_k) = \frac{c_{jk}}{16\pi}\lambda^2 m_{\tilde{\nu}_i}, \tag{2}$$

where c_{jk} is a color factor, and λ ($= \lambda_{ijk}$ or λ'_{ijk}) is the coupling to the final-state $f_j f_k$. The width is fairly narrow; for example, if only λ'_{i11} and one λ_{ijk} are large, then for respective values of $1/2$ and 1, the width is 3.5% of the mass (this can be compared to the Z boson, whose width is 2.8% of its mass [24]).

A range of indirect limits exist on λ'_{i11} [25], and generally depend on other supersymmetric parameters. A typical set of limits comes from the ratio of $\Gamma(\pi \to e\nu)/\Gamma(\pi \to \mu\nu)$ or $\Gamma(\tau \to \pi\nu)/\Gamma(\pi \to \mu\nu)$: $\lambda'_{i11} < a_i m_{\tilde{d}}/\text{TeV}$, where $a_1 = 0.26$, $a_2 = 0.59$, and $a_3 = 1.2$. For reasonable values of $m_{\tilde{d}}$ ($0.2-1$ TeV), these limits allow significant production rates with a relatively narrow decay width.

B. Z' Vector Bosons

Many models predict a new electroweak-scale U(1) gauge symmetry [26, 27, 28, 29], which would have an associated Z' gauge boson. A useful test model is a superstring-inspired grand unified theory with $E_8 \times E_8'$ gauge structure [30]. In this model, the E_8' group is a hidden sector that breaks supersymmetry, and the E_8 group is broken to $E_6 \times$SU(3) by the compactification of extra dimensions [31]. Each generation of matter particles fits in a fundamental 27 representation of E_6; thus, before E_6 is broken, each SM generation is just a single field distinguished by its E_6 charge.

The range of options for breaking E_6 to the SM gauge structure allows a variety of phenomena [16]. A symmetry-breaking proceeding through SO(10)×U(1) to SU(4)$_C$×SU(2)$_L$×SU(2)$_R$×U(1)$_{B-L}$ restores parity conservation and provides for the seesaw mechanism for small neutrino masses. Alternatively, the breaking can proceed through SO(10)×U(1)$_\psi$ to SU(5)×U(1)$_\chi$×U(1)$_\psi$, producing two new U(1) gauge groups. At a high mass scale, the SU(5) can be broken to the SM gauge groups and one of the extra U(1) gauge groups can be broken, potentially leaving one non-SM U(1)$'$ at the electroweak scale. Taking this U(1)$'$ to be a linear combination of U(1)$_\psi$ and U(1)$_\chi$,

$$\mathrm{U}(1)' = \mathrm{U}(1)_\psi \cos\theta + \mathrm{U}(1)_\chi \sin\theta, \tag{3}$$

a generic U(1)$'$ can be expressed in terms of θ [32].

Scanning the θ parameter space gives models with distinct phenomena. The secluded U(1)$'$ ($\theta = \pi - \tan^{-1}\sqrt{27/5}$) is mediated by a Z'_{sec} boson whose mass results from the vacuum expectation value of a scalar field with no SM charge [33]. For $\theta = -\tan^{-1}\sqrt{1/15}$, the right-handed neutrino has no charge in the extended gauge group (SU(3)$_c$×SU(2)$_L$×U(1)$_Y$×U(1)$_N$), and is thus sterile [34]. The breaking of E_6 directly to the SM groups plus U(1)$_\eta$ corresponds to $\theta = \tan^{-1}\sqrt{3/5}$. If the breaking proceeds through an extra SU(2)$_I$ group (instead of SU(2)$_R$), then the W' and Z' bosons of the new group have zero electromagnetic charge.

More general classes of models have also been considered, with the constraint of anomaly cancellation to produce a consistent theory [35]. Under the assumption of the SM Higgs mechanism for generating fermion masses, a general class of models has U(1)$'$ charge $B - xL$, where B (L) is baryon (lepton) number (and the right-handed neutrino charge is fixed to -1). Allowing for non-SM mass generation but considering only SM particles for anomaly cancellation gives U(1)$'$ charges 1/3, $x/3$, $(2-x)/3$, -1, $-(2+x)/3$, and $(-4+x)/3$ for the states q_L, u_R, d_R, l_L, e_R, and ν_R, respectively. This model is referred to as $q + xu$ and includes the case of $B - L$ symmetry for $x = 1$. Two additional model classes arise when two non-SM fermions are added to the theory. One is referred to as $d - xu$ and has charges of 0, 1/3, and $-x/3$ for q_L, d_R, and u_R, respectively. The other, $10 + x\bar{5}$, has fermions in the 10 representation of the SU(5) grand unified group with the $U(1)'$ charge 1/3, and fermions in the $\bar{5}$ representation with charge $x/3$.

In general, couplings of the new Z' boson to SM particles are smaller than those of the Z boson in the SM. However, the new Z' boson could decay into the non-SM particles that are part of the 27 representation of E_6. If decay to all of these particles is possible, the Z' boson width could be $\approx 5\%$ of its mass [36]. Even in this extreme case, the Z' boson would appear as a narrow resonance.

C. Graviton Resonances

It has been suggested that the apparent difference between the scales of gravity and electroweak symmetry-breaking is due to the presence of at least one unobserved spatial dimension [8, 17]. The spread of the gravitational field into the extra dimension(s) weakens the strength of gravity in the observed dimensions. Closing the gap between the electroweak and Planck scales requires either the number or the size of the extra dimensions to be large, if they are flat.

Recently, Randall and Sundrum have proposed a model that removes the scale hierarchy using one small extra dimension [17]. This can be accomplished with a warped dimension separating the SM brane from the gravity brane, resulting in a metric of the form:

$$ds^2 = e^{-2kr\phi}\eta_{\mu\nu}dx^\mu dx^\nu - r^2 d\phi^2, \tag{4}$$

where r is the compactification radius, and k^2 and $\phi = [-\pi, \pi]$ are the spacetime curvature and coordinate in the extra dimension, respectively. The curvature is of the order of M_{Pl}^2, where $M_{Pl} = G_N^{-1/2} \sim 10^{19}$ GeV is the Planck scale on the 4-dimensional spacetime and G_N is the Newtonian gravitational constant. For a string theory with $\mathcal{O}(1)$ couplings, $k/M_{Pl} \sim 0.01$ [18].

Due to the spacetime warping, distances are exponentially larger on the gravity brane, resulting in a large gravitational field flux on this brane. The gravitational force for an observer on the SM brane appears as:

$$F \sim m_1 m_2/(M_{EW}^2 e^{2kr\pi} R^2), \tag{5}$$

where R is the distance between masses m_1 and m_2 in the three large spatial dimensions. Thus, $kr \sim 12$ reproduces the observed weakness of gravity and there are no large hierarchies in the model. In terms of the gravitational quantum, the wave function of the massless graviton state is localized on the gravity brane and exponentially suppressed on the SM brane.

Graviton excitations are localized on the SM brane and are thus expected to have mases m_n at the electroweak scale,

$$m_n = kx_n e^{-kr\pi}, \tag{6}$$

where x_n are $\mathcal{O}(1)$ roots of a Bessel function and $ke^{-kr\pi}$ is of the order of the electroweak scale. The resonance width is proportional to $(k/M_{Pl})^2$, and is less than a few percent for $k/M_{Pl} \leq 0.1$.

III. COLLIDER SEARCHES FOR NEUTRAL RESONANCES

The most stringent direct limits on new neutral resonances come from searches at the Tevatron. Run II searches at the CDF and D0 experiments have probed resonance decays to pairs of electrons [37, 38, 39, 40, 41, 42], muons [39, 41, 42], taus [42, 43, 44, 45], light quarks [42, 46], top quarks [42, 47], gluons [42, 46], photons [40, 41, 42, 48], and W [49] and Z [50] bosons. The most sensitive searches use long-lived final-state particles, while other searches cover parameter space where couplings to long-lived particles are suppressed.

Searches for a resonance decaying to a pair of stable particles typically probe the reconstructed invariant mass distribution for evidence of a narrow peak, with the peak width determined primarily by detector resolution. Because detector resolutions increase with increasing mass, the expected peak width also increases. This complication usually results in search windows that change as a function of mass, with the window causing some loss of acceptance. A recent CDF search [11] uses templates to fit the full dimuon inverse invariant mass spectrum for new resonances, avoiding the acceptance loss from a search window. In addition, the inverse mass distribution has approximately constant resolution, simplifying the search.

A complement to the invariant mass distribution is the angular distribution of the final-state particles, which can be used to separate a signal from the SM background and to determine the spin of the new resonance. CDF has performed a search in the dielectron final state using the $\cos\theta^*$ distribution [12], where θ^* is the angle between the electron and the incoming quark in the boson rest frame [51].

A. CDF Dimuon Search

Currently, the CDF dimuon analysis of 2.3 fb^{-1} of $p\bar{p}$ collision data is the most sensitive search for neutral resonances over most of the probed parameter space. The search uses a parametric simulation to model the detector response and resolution for muons, calibrated using known resonances. After normalizing the SM inverse mass spectrum to the Z boson peak, the data are fit as functions of the number of new-neutral-resonance events above background and the resonance pole mass. No statistically significant excess above the background is observed, and limits are set for the various test models.

1. Detector Alignment and Calibration

In the CDF search, muon momenta are measured with the central outer tracker (COT) [52], a wire drift chamber embedded in a 1.4 T magnetic field covering $|\eta| < 1$ and radii 43 cm to 133 cm [53]. The reconstructed tracks are constrained to originate from the time-averaged transverse beam collision coordinate, significantly improving momentum measurement resolution. Calorimeters and a muon detector system at large radii from the beam line are used for muon identification and event triggering.

To minimize bias and optimize the detector resolution (and thus the statistical significance of a narrow resonance), a detailed alignment of the COT is performed [54]. The alignment uses cosmic-ray muons reconstructed as a single track through both sides of the nominal collision point [55]. With 96 radial wire layers in the COT, any given two-sided track has up to 192 measurement points. The 96 layers are divided into 8 superlayers of 12 wires each, with each superlayer containing enough 2 cm wide cells to cover the azimuth. The first stage of the alignment allows a rotation and a shift of each cell, such that the mean residual of hits in any given cell is statistically consistent with zero (with a precision of a few microns).

After the individual cell alignment, a global correction to the wire shape between endplates is derived as a function of ϕ and radius. The shape is determined by the gravitational sag from the weight of the wire, and by the electrostatic deflection from the local electric field. The nominal correction to the wire shape due to these effects is further modified with an empirical correction function derived from measured biases between the two separately fit sides of the cosmic-ray tracks.

A final correction to the track curvature is applied after the track reconstruction. The correction is derived from the difference in the ratio of calorimeter energy to track momentum for positrons and electrons, as functions of ϕ and $\cot\theta$ [53].

The momentum scale is calibrated by tuning the measured J/ψ, Υ, and Z boson masses to their precisely known values. Individual hit resolutions of 150 microns are determined from the observed width of the $\Upsilon \to \mu\mu$ peak, consistent with hit residuals of muons from Z boson decays. The transverse beam profile is modelled as a gaussian with a size set by the observed width of the $Z \to \mu\mu$ mass peak measured with beam-constrained tracks.

2. Inverse Mass Scan

Muon momenta transverse to the beam line are determined from a measurement of the reconstructed track curvature c. The Lorentz force $q\vec{v} \times \vec{B}$ causes a helical trajectory of the muon, resulting in a transverse momentum:

$$p_T = eBR, \tag{7}$$

where R is the radius of curvature and B is the magnitude of the magnetic field.

The resolution on the track curvature ($c \equiv R^{-1}/2$ at CDF) can be derived from the individual hit resolutions. Taking as an example a muon produced with no impact parameter at $\phi = 0$, its position at a given radius r is $(r\cos\phi, r\sin\phi)$. Using the equation of the track circle, $x^2 + (y - R)^2 = R^2$, the curvature is $c = \sin\phi/r$ and its resolution due to a measured hit is $\delta c = \cos\phi\,\delta\phi/r$. The partial derivative of the curvature with respect to the hit resolution $\delta D = r\delta\phi$ is then

$$\delta c/\delta D = (1 - c^2 r^2)^{1/2}/r^2. \tag{8}$$

For muons with small curvature (large momentum), the resolution is effectively independent of curvature and improves with the square of the detector radius.

Defining the reconstructed muon energies to be E_1 and E_2, and their opening angle to be Θ, the measured mass can be expressed as:

$$m = [2E_1 E_2(1 - \cos\Theta)]^{1/2}. \tag{9}$$

The dominant contribution to the mass resolution comes from the momentum measurement, since the angular resolution is negligible by comparison. A high-mass resonance is predominantly produced with a relatively small transverse boost, resulting in muons with similar transverse momenta. Then, $m \propto p_T$, or $1/m \propto c$. Thus, a new narrow resonance would have an approximately constant width in the reconstructed $1/m$ distribution of central muons.

The search in a constant-width variable simplifies the analysis. A distribution with uniform binning can be visually scanned for resonances. Taking bin widths sufficiently narrow with respect to the resolution allows a template fit for a resonance centered on each bin, with the step size an equal fraction of the peak width throughout the distribution. This procedure optimizes the scan of the $1/m$ distribution.

At CDF, the inverse mass resolution is 17% TeV^{-1}, with an additional contribution from multiple scattering at low mass. At 100 GeV, the total resolution is about 30% smaller than the intrinsic width of the Z boson. Thus, the width of the new resonance could noticeably broaden the peak at low mass. However, the relative resolution increases linearly with increasing mass, while the relative instrinsic width remains constant, so for most resonances the detector resolution will dominate above a few hundred GeV.

In the CDF analysis, the search region is 35 bins of $m^{-1} < 10$ TeV^{-1}, resulting in an expected peak width of about 3 bins due to detector resolution. The 70-100 GeV mass range is used to normalize the expected background, effectively removing systematic uncertainties due to luminosity, background cross section, and trigger and muon identification efficiencies. For each probed inverse mass bin, a template of combined signal and background is compared to the data to determine the number of signal events that maximizes the log Poisson likelihood.

The template fit adds acceptance outside of the usual mass window, particularly at masses near the kinematic threshold. While the template neglects interference between the new resonance and Z and γ bosons, any interference has a small effect on the search because the resonance is narrow and has a small cross section [35].

3. Backgrounds

Dimuon production at a hadron collider occurs predominantly through the Drell-Yan process of Z/γ^* production. This process has been calculated at next-to-next-to-leading order (NNLO) in α_s [35] and next-to-leading order (NLO)

in α_{EW} [56] at the Tevatron, and is thus well understood theoretically. Since the CDF analysis normalizes the background to the Z boson peak, the shape of the inverse mass distribution is the important theoretical input. Over the probed mass region, the ratio of NNLO to leading order (LO) predictions have an $\approx 10\%$ variation. The difference between NLO and NNLO predictions is taken as a systematic uncertainty and increases from zero at 91 GeV (the normalization mass) to 9% for a mass of 1 TeV. A more important systematic uncertainty at 1 TeV comes from uncertainties on the parton distribution functions (PDFs). At this mass, the valence (anti-)quarks must have a large fraction of the (anti-)proton's momentum. The uncertainty obtained from a comparison of CTEQ [57] PDFs fit using LO and NLO inputs increases with mass to approximately 16% at 1 TeV. No NLO α_{EW} correction is applied, and a 3% uncertainty at 1 TeV is incorporated to cover its neglect.

A background relevant at high mass arises from hadrons decaying to muons in the COT, where the track is misreconstructed as a nearly straight line. The misreconstruction occurs via a track kink at the decay vertex or other incorrectly assigned hits in the inner superlayers. This background is reduced by requiring each muon's COT hit pattern and track fit χ^2 to be consistent with a well-measured track resulting from the collision vertex. The small residual background is estimated using dimuons with the same charge, which are assumed to arise from misidentification or other non-prompt sources.

W boson pairs produced either directly or through top quark decays contribute to the dimuon sample when both W bosons decay to $\mu\nu$. These backgrounds have been calculated to NLO in α_s [58, 59] and are only relevant at high mass.

A final potential background arises from cosmic-ray muons passing through the detector. These muons can have high energies and thus contribute to the background at high mass. At CDF the cosmic-ray background is effectively eliminated by the two-sided track fit used to identify cosmic-ray muons in the COT [55].

4.   Signal Cross Sections and Acceptance

Cross sections for sneutrino production have been calculated at NLO in α_s [60]. If there is CP conservation in the sneutrino sector, the anti-sneutrino and sneutrino cross sections will be the same; this assumption is made in the CDF analysis. Z'-boson and Randall-Sundrum-graviton cross sections are determined from PYTHIA [61] with an NNLO α_s correction factor applied [35], and the appropriate couplings are used for the various E_6 models [62].

In the CDF analysis, acceptance is calculated as a function of spin and inverse mass. For 1 TeV resonances, which are produced with relatively little longitudinal momenta, the acceptance for observing two central muons is $\approx 40\%$. At 100 GeV, the larger average longitudinal boost reduces the acceptance for the CDF central muon and tracking chambers, resulting in an acceptance of $\approx 15\%$. A relative uncertainty of 3% is estimated from comparisons of the parametric and GEANT-based detector simulations. A study of $Z \to \mu\mu$ events shows the momentum dependence of the muon identification efficiency to be well modelled by the simulation.

5.   Results and Limits

The observed dimuon invariant mass spectrum (Fig. 2) shows no evidence for a new neutral resonance. This can be clearly seen in the error-weighted difference between observation and expectation (Fig. 3). A narrow resonance would appear as a significant excess in one bin, with additional excesses in neighboring bins. The most significant observed excess occurs at the lowest probed mass in the search, 103 GeV. An ensemble of simulated experiments gives a 6.6% probability of finding a more significant excess anywhere in the search region from a background fluctuation.

The results are translated into cross-section limits for new resonance production (Figs. 4-6), and then into mass limits for specific models (Table I). The mass limits are the highest of any search, except for models with weak couplings. For such couplings, the probed mass range is lower and the recent CDF dielectron search [37] has better sensitivity, since the CDF calorimeter has broader coverage in η. The lower the resonance mass, the larger the average boost in the beam direction, and the larger the average rapidities of the leptons. The dielectron analysis thus has better acceptance and sensitivity at these masses.

B.   CDF Dielectron Search

The CDF dielectron search in 0.45 fb^{-1} of $p\bar{p}$ collision data is the only hadron-collider search for Z' bosons to use the dilepton angular information. The search parametrizes the detector response in the $(m_{ee}, \cos\theta^*)$ plane and distinguishes the SM and Z'-boson hypotheses using the observed distribution in this plane. The data are consistent with the SM so limits are set on Z' bosons in a generalized model parameter space.
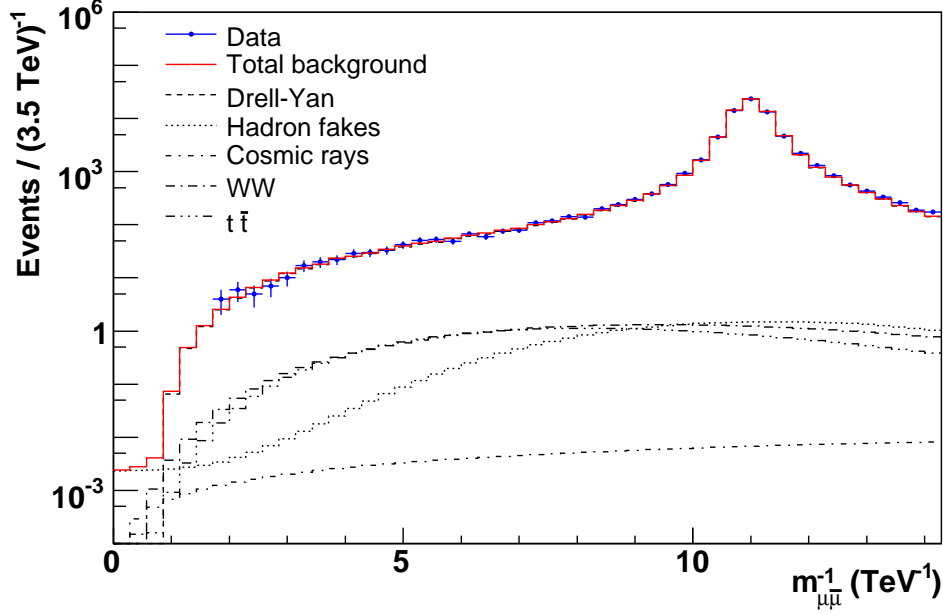
FIG. 2: The inverse invariant dimuon mass for data and expected background. The Z boson peak is prominent at ≈ 11 TeV^{-1}, and a new resonance would appear as a similar (narrower) peak in the sloping region on the left.
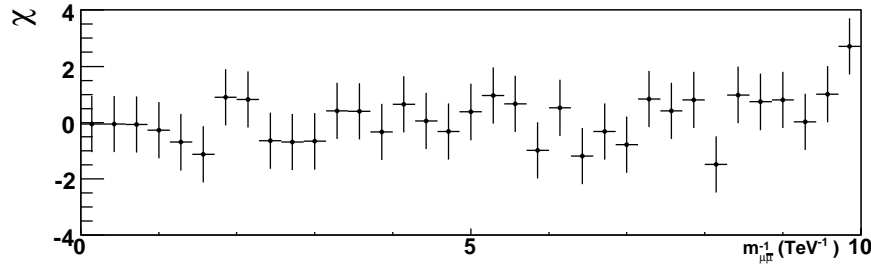

FIG. 3: The difference between data and expected background, divided by the statistical uncertainty. The data are consistent with the background expectation; the most significant excess appears in the rightmost bin, corresponding to a mass of 103 GeV.

1. Two-dimensional $(m_{ee}, \cos\theta^*)$ Scan

The scattering amplitude for the $f\bar{f} \rightarrow e^-e^+$ process is [63]

$$A_{ij} = A(f_i\bar{f} \rightarrow e_j^- e^+) = -Qe^2 + \frac{\hat{s}}{\hat{s}-m_Z^2+im_Z\Gamma_Z}C_i^Z(f)C_j^Z(e) +$$
$$\frac{\hat{s}}{\hat{s}-m_{Z'}^2+im_{Z'}\Gamma_{Z'}}C_i^{Z'}(f)C_j^{Z'}(e), \tag{10}$$

where i and j are the fermion helicities (L, R), Q is the electromagnetic charge of fermion f, $C_{i,j}^{Z,Z'}(f)$ are the fermion couplings to the Z and Z' bosons, m_Z (Γ_Z) and $m_{Z'}$ ($\Gamma_{Z'}$) are the respective Z and Z' boson masses (widths), and $\hat{s}$ is the squared center-of-mass energy of the collision. Using this amplitude, the differential angular cross section is

$$\frac{d\sigma}{d\cos\theta^*} = \frac{1}{128\pi\hat{s}}[(|A_{LL}|^2 + |A_{RR}|^2)(1 + \cos\theta^*)^2 + (|A_{LR}|^2 + |A_{RL}|^2)(1 - \cos\theta^*)^2]. \tag{11}$$

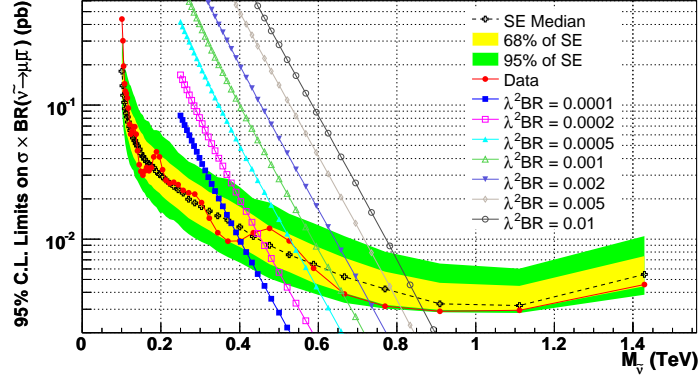A Z' boson with non-zero couplings to quarks and electrons alters the SM $\cos\theta^*$ distribution.

FIG. 4: The cross section limits for a new spin-0 resonance, and the theoretical predictions for sneutrino production for various values of the coupling squared ($\lambda'^2_{i11} \equiv \lambda^2$) times the branching ratio to dimuons.
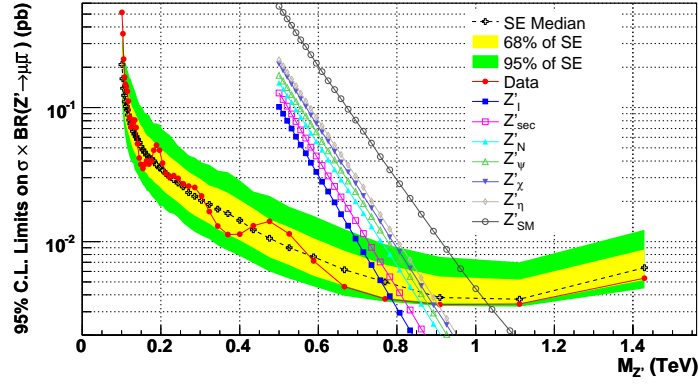

FIG. 5: The cross-section limits for a new spin-1 resonance, and the theoretical predictions for Z' bosons with the same couplings to fermions as the Z boson (Z'_{SM}), and in various E_6-inspired models.
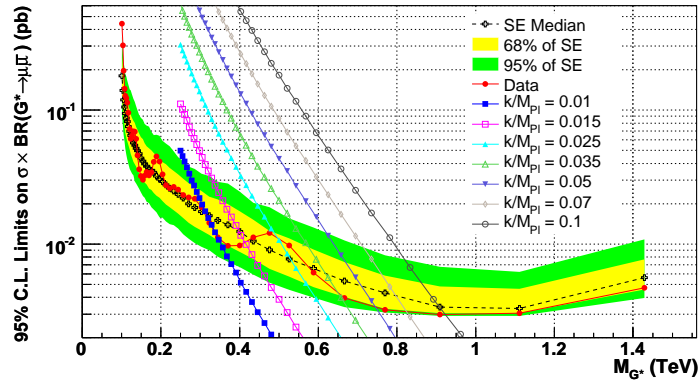

FIG. 6: The cross-section limits for a new spin-2 resonance, and the theoretical predictions for R-S gravitons for various values of k/M_{Pl}.

TABLE I: 95% C.L. lower mass limits, in GeV, for sneutrinos, Z' bosons, and gravitons with various model parameters. The Z'_{SM} boson has the same couplings to fermions as the Z boson.

$\tilde{\nu}$	$\tilde{\nu}$	Z'	Z'	RS graviton	graviton
$(\lambda'_{i11})^2 \cdot BR$ mass limit		model	mass limit	k/M_{Planck}	mass limit
0.0001	397	Z'_I	789	0.01	293
0.0002	441	Z'_{sec}	821	0.015	409
0.0005	541	Z'_N	861	0.025	493
0.001	662	Z'_ψ	878	0.035	651
0.002	731	Z'_χ	892	0.05	746
0.005	810	Z'_η	904	0.07	824
0.01	866	Z'_{SM}	1030	0.1	921

The CDF search probes the $(m_{ee}, \cos\theta^*)$ plane in (10 GeV, 0.25) bins using a look-up table from the full detector simulation to determine the acceptance in each bin. The Z' boson signal hypothesis, including interference with the Drell-Yan process, is compared to SM Z/γ^* boson production through a likelihood ratio for the two hypotheses in the search region of $m_{ee} > 200$ GeV. The processes are modelled with PYTHIA [61] and a mass-dependent NNLO correction factor [35].

In the search region CDF estimates the following SM backgrounds in 0.45 fb^{-1} of data: 80 Drell-Yan events; 28 events with a jet misreconstructed as an electron (dijet and W + jet); and 7 diboson (WW and WZ) events. The misreconstructed-jet events are estimated by applying a jet-to-electron misreconstruction rate to all jets in events with one reconstructed electron and at least one jet. Diboson events are estimated with PYTHIA and their theoretical cross sections [58].

2. Results

The 120 observed events in the search region are consistent with the 115^{+16}_{-19} expected background events in the two-dimensional $(m_{ee}, \cos\theta^*)$ plane. The projections along the m_{ee} and $\cos\theta^*$ axes are shown in Figs. 7 and 8.
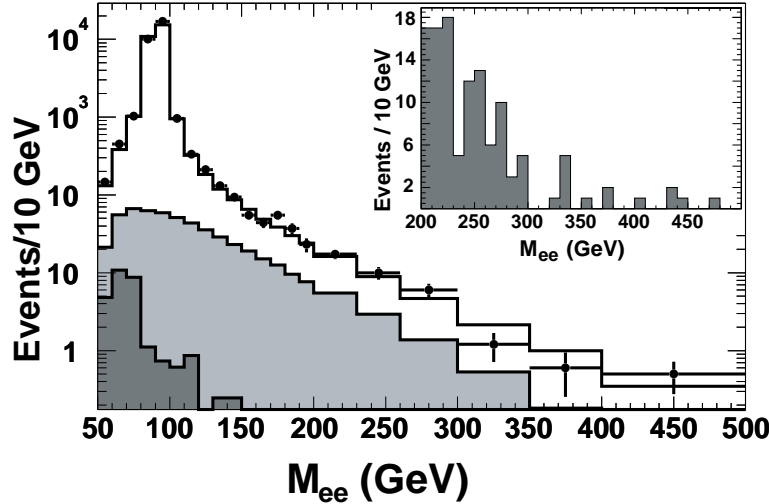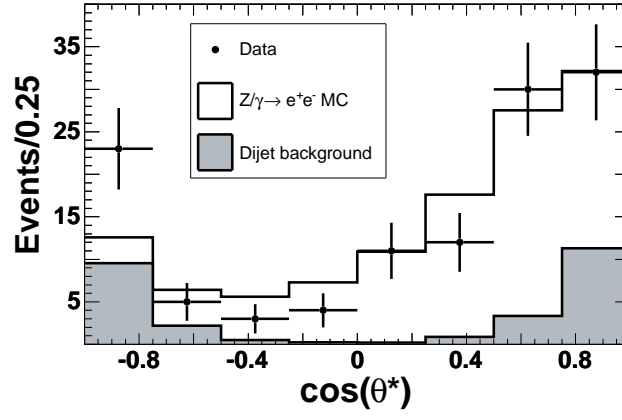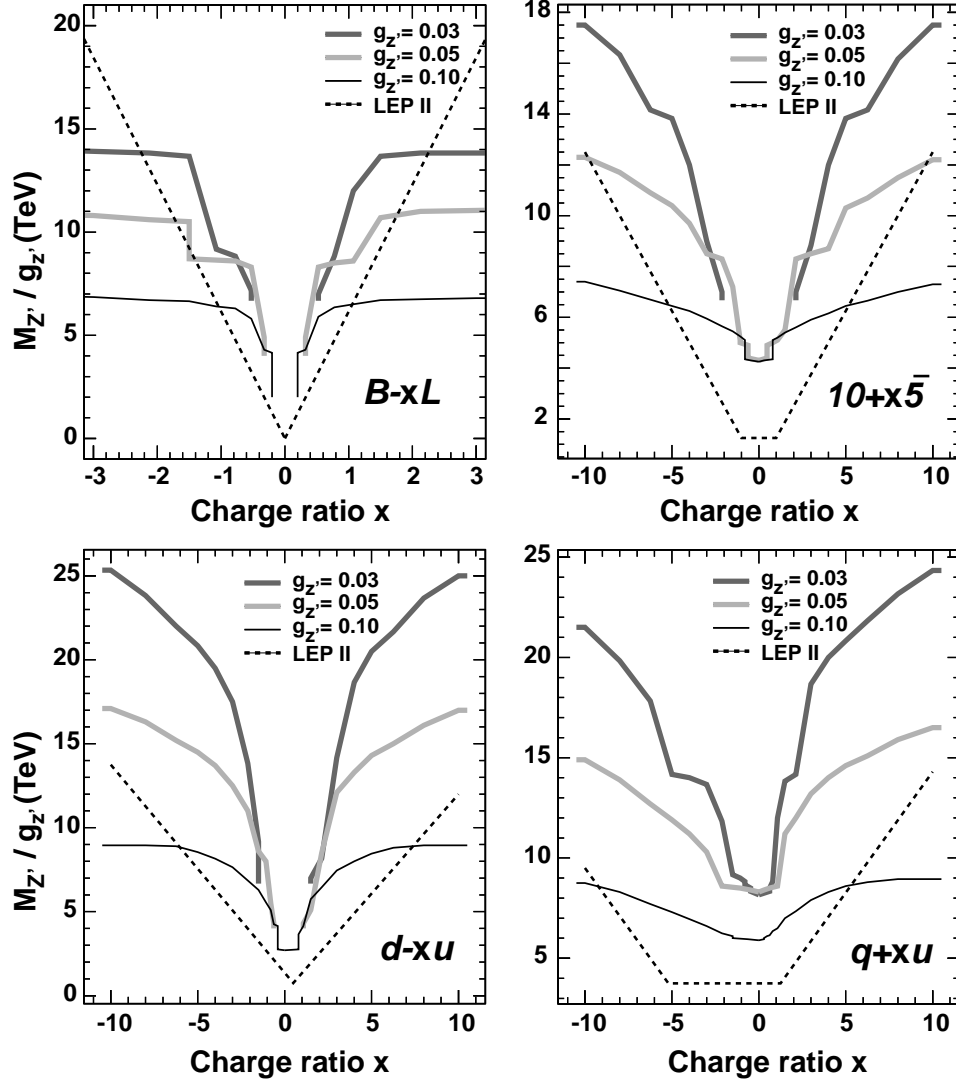

FIG. 7: The invariant dielectron mass for data and expected background. The inset shows the data events in the search region $m_{ee} > 200$ GeV.

From the comparison of SM and Z' hypotheses, limits are set on the masses and couplings of Z' bosons. The mass limits range from 675 GeV for Z'_{sec} to 860 GeV for Z'_{SM}. For the generalized models $B - xL$, $q + xu$, $d - xu$, and $10 + x\bar{5}$, limits are set in the two-dimensional plane of $(x, M_{Z'}/g_{Z'})$ for several values of $g_{Z'}$ (Fig. 9). The limits extend to smaller values of $|x|$ and $g_{Z'}$ than those from LEP II.

FIG. 8: The $\cos\theta^*$ distribution in $m_{ee} > 200$ GeV search region.

FIG. 9: Limits from the CDF dielectron search in the generalized $(x, M_{Z'}/g_{Z'})$ plane for several values of $g_{Z'}$. Values below the curves are excluded, and LEP II limits are shown for comparison.

IV.   FUTURE SEARCHES

The full Run II data sets are expected to be a factor of 4 larger than that used in the CDF dimuon analysis. The highest current mass limits are at the edge of a steeply falling parton-luminosity curve and will not significantly increase. However, there is ample opportunity to see hints of a weakly-coupled new resonance at a mass below the kinematic threshold using the full CDF and D0 data sets. With the higher energy collisions soon expected from the LHC, the highest probed mass could increase by a factor of 3 or more [10]. Thus, neutral resonance searches will continue to provide significant discovery potential into the future.

The technique applied to the CDF dimuon search can be extended to searches in other final states. For example, at high mass the calorimetric measurement of electrons and photons has a fractional energy resolution that is constant in energy because the calorimeter sampling term becomes negligible in comparison. Since $\delta \ln m = \delta m/m$, a new resonance decaying to electron pairs will have a constant peak width in the $\ln m$ distribution. This is not affected by the fractional intrinsic width, which is also constant in mass. For resonances decaying to quarks and gluons, the optimal distribution depends on the calorimeter. At low energy the resolution is proportional to $\sqrt{E}$, so the fractional resolution improves with increasing energy. In this case resonances will have constant width in the $\sqrt{E}$ distribution. At sufficiently high mass, however, the intrinsic width and constant fractional resolution term will become dominant, in which case resonances will have constant width in $\ln m$.

The angular distributions of the final-state particles included in the Z'-boson search at CDF have also been used by D0 to search for graviton production [64, 65]. Optimally, an unbinned likelihood can be performed for each spin hypothesis, using the full matrix-element and resolution information on an event-by-event basis. This technique has been applied to Higgs-boson and top-quark searches [49, 66] and measurements [67] at the Tevatron. For a high-mass resonance search, a modest gain in sensitivity is expected beyond a two-dimensional $(m_{ll}, \cos\theta^*)$ fit.

Acknowledgments

[1] J. J. Aubert *et al.*, *Phys. Rev. Lett.* **33**, 1404 (1974); J.-E. Augustin *et al.*, Phys. Rev. Lett. **33**, 1406 (1974).

[2] S. L. Glashow, J. Iliopoulos, and L. Maiani, *Phys. Rev. D* **2**, 1285 (1970).

[3] G. Arnison *et al.* (UA1 Collaboration), *Phys. Lett. B* **126**, 398 (1983); P. Bagnaia *et al.* (UA2 Collaboration), *Phys. Lett. B* **129**, 130 (1983).

[4] S. Glashow, *Nucl. Phys.* **22**, 579 (1967); S. Weinberg, *Phys. Lett.* **12**, 132 (1967); A. Salam, *Elementary Particle Physics*, N. Svartholm ed., 367 (1968).

[5] S. W. Herb *et al.*, *Phys. Rev. Lett.* **39**, 252 (1977).

[6] F. Englert and R. Brout, *Phys. Rev. Lett.* **13**, 321 (1964); P. Higgs, *Phys. Rev. Lett.* **13**, 508 (1964); G. Guralnik, C. R. Hagen, and T. W. B. Kibble, *Phys. Rev. Lett.* **13**, 585 (1964).

[7] Yu. A. Gol'fand and E. P. Likhtman, *JETP Lett.* **13**, 323 (1971); D. V. Volkov and V. P. Akulov, *Phys. Lett. B* **46**, 109 (1973); J. Wess and B. Zumino, *Nucl. Phys. B* **70**, 39 (1974).

[8] N. Arkani-Hamed, S. Dimopoulos, and G. Dvali, *Phys. Lett. B* **429**, 263 (1998).

[9] J. C. Pati and A. Salam, *Phys. Rev. D* **10**, 275 (1974); R. N. Mohapatra and J. C. Pati, *Phys. Rev. D* **11**, 566 (1975); G. Senjanovic and R. N. Mohapatra, *Phys. Rev. D* **12**, 1502 (1975).

[10] G. Aad *et al.* (ATLAS Collaboration), *arXiv:0901.0512* (2009); D. Bourilkov, *arXiv:0807.4960v1* (2008).

[11] T. Aaltonen *et al.* (CDF Collaboration), *Phys. Rev. Lett.* **102**, 091805 (2009).

[12] A. Abulencia *et al.* (CDF Collaboration), *Phys. Rev. Lett.* **96**, 211801 (2006).

[13] S. Kraml *et al.*, *arXiv:hep-ph/0608079v1* (2006).

[14] S. Dimopoulos and L. J. Hall, *Phys. Lett. B* **207**, 210 (1987); S. Dimopoulos *et al.*, *Phys. Rev. D* **41**, 2099 (1990).

[15] P. Fayet, *Phys. Lett. B* **69**, 489 (1977); A. Davidson, *Phys. Rev. D* **20**, 776 (1979).

[16] P. Langacker, *arXiv:0801.1345v2* (2008).

[17] L. Randall and R. Sundrum, *Phys. Rev. Lett.* **83**, 3370 (1999).

[18] H. Davoudiasl, J. L. Hewett, and T. G. Rizzo, *Phys. Rev. Lett.* **84**, 2080 (2000).

[19] S. Borgani, A. Masiero, and M. Yamaguchi, *Phys. Lett. B* **386**, 189 (1996); F. Takayama and M. Yamaguchi, *Phys. Lett B* **485**, 388 (2000); S. K. Gupta, P. Konar, and B. Mukhopadhyaya, *Phys. Lett. B* **606**, 384 (2005); D. A. Sierra, D. Restrepo, and O. Zapata, *arXiv:0907.0682v2* (2009).

[20] I. Hinchcliffe and T. Kaeding, *Phys. Rev. D* **47**, 279 (1993); A. Yu. Smirnov and F. Vissani, *Phys. Lett. B* **380**, 317 (1996).

[21] L. E. Ibáñez and G. G. Ross, *Nucl. Phys. B* 368, 3 (1992).

[22] V. Barger, W.-Y. Keung, and R. J. N. Phillips, *Phys. Lett. B* **364**, 27 (1995).
[23] We use natural units where $c \equiv \bar{h} \equiv 1$ throughout.
[24] S. Schael *et al.* (ALEPH, DELPHI, L3, OPAL, and SLD Collaborations), *Phys. Rep.* **427**, 257 (2006).
[25] R. Barbier *et al.*, *Phys. Rep.* **420**, 1 (2005).
[26] C. T. Hill and E. H. Simmons, *Phys. Rep.* **381**, 235 (2003).
[27] N. Arkani-Hamed, A. G. Cohen, and H. Georgi, *Phys. Lett. B* **513**, 232 (2001); T. Han, H. E. Logan, B. McElrath, and L.-T. Wang, *Phys. Rev. D* **67**, 095004 (2003).
[28] M. Cvetič and P. Langacker, *Phys. Rev. D* **54**, 3570 (1996); M. Cvetič *et al.*, *Phys. Rev. D* **56**, 2861 (1997).
[29] J. L. Hewett and T. G. Rizzo, *Phys. Rep.* **183**, 193 (1989).
[30] M. B. Green and J. H. Schwarz, *Phys. Lett. B* **149**, 117 (1984); D. Gross, J. A. Harvey, E. Martinec, and R. Rohm, *Phys. Rev. Lett.* **54**, 502 (1985); *ibid.*, *Nucl. Phys. B* **256**, 253 (1985); *ibid.*, *Nucl. Phys. B* **267**, 75 (1986).
[31] P. Candelas, G. T. Horowitz, A. Strominger, and E. Witten, *Nucl. Phys. B* **258**, 46 (1985); E. Witten, *Nucl. Phys. B* **258**, 75 (1985); *ibid.*, *Phys. Lett. B* **149**, 351 (1984).
[32] D. London and J. L. Rosner, *Phys. Rev. D* **34**, 1530 (1986).
[33] J. Erler, P. Langacker, and T. Li, *Phys. Rev. D* **66**, 015002 (2002).
[34] E. Ma, *Phys. Lett. B* **380**, 286 (1996).
[35] M. Carena, A. Daleo, B. A. Dobrescu, and T. M. P. Tait, *Phys. Rev. D* **70**, 093009 (2004).
[36] J. Kang and P. Langacker, *Phys. Rev. D* **71**, 035014 (2005).
[37] T. Aaltonen *et al.* (CDF Collaboration), *Phys. Rev. Lett.* **102**, 031801 (2009).
[38] T. Aaltonen *et al.* (CDF Collaboration), *Phys. Rev. Lett.* **99**, 171802 (2007).
[39] A. Abulencia *et al.* (CDF Collaboration), *Phys. Rev. Lett.* **95**, 252001 (2005).
[40] V. M. Abazov *et al.* (D0 Collaboration), *Phys. Rev. Lett.* **100**, 091802 (2008).
[41] V. M. Abazov *et al.* (D0 Collaboration), *Phys. Rev. Lett.* **95**, 091801 (2005).
[42] T. Aaltonen *et al.* (CDF Collaboration), *Phys. Rev. D* **79**, 011101 (2009).
[43] V. M. Abazov *et al.* (D0 Collaboration), *Phys. Rev. Lett.* **101**, 071804 (2008); V. M. Abazov *et al.* (D0 Collaboration), *Phys. Rev. Lett.* **97**, 121802 (2006).
[44] D. Acosta *et al.* (CDF Collaboration), *Phys. Rev. D* **72**, 072004 (2005).
[45] D. Acosta *et al.* (CDF Collaboration), *Phys. Rev. Lett.* **95**, 131801 (2005).
[46] T. Aaltonen *et al.* (CDF Collaboration), *Phys. Rev. D* **79**, 112002 (2009).
[47] T. Aaltonen *et al.* (CDF Collaboration), *Phys. Rev. D* **77**, 051102(R) (2008); T. Aaltonen *et al.* (CDF Collaboration), *Phys. Rev. Lett.* **100**, 231801 (2008); V. M. Abazov *et al.* (D0 Collaboration), *Phys. Lett. B* **668**, 98 (2008).
[48] T. Aaltonen *et al.* (CDF Collaboration), *Phys. Rev. Lett.* **99**, 171801 (2007); V. M. Abazov *et al.* (D0 Collaboration), *Phys. Rev. Lett.* **102**, 231801 (2009).
[49] T. Aaltonen *et al.* (CDF Collaboration), *Phys. Rev. Lett.* **102**, 021802 (2009); A. Abulencia *et al.* (CDF Collaboration), *Phys. Rev. Lett.* **97**, 081802 (2006); V. M. Abazov *et al.* (D0 Collaboration), *Phys. Rev. Lett.* **96**, 011801 (2006).
[50] T. Aaltonen *et al.* (CDF Collaboration), *Phys. Rev. D* **78**, 012008 (2008).
[51] J. C. Collins and D. E. Soper, *Phys. Rev. D* **16**, 2219 (1977).
[52] T. Affolder *et al.*, *Nucl. Instrum. Methods Phys. Res. A* **526**, 249 (2004).
[53] CDF uses a cylindrical coordinate system in which $+z$ points in the direction of the proton beam (east), ϕ is the azimuthal angle and r is the radius from the center of the detector. The rapidity $y = -\frac{1}{2}\ln[(E - p_z)/(E + p_z)]$ is additive under Lorentz boosts along the z axis and reduces to the pseudorapidity $\eta = -\ln[\tan(\theta/2)]$ for massless particles, where θ is the polar angle with respect to the z axis.
[54] T. Aaltonen *et al.* (CDF Collaboration), *Phys. Rev. D* **77**, 112001 (2008).
[55] A. V. Kotwal, H. K. Gerberich, and C. Hays, *Nucl. Instrum. Methods Phys. Res. A* **506**, 110 (2003).
[56] U. Baur *et al.*, *Phys. Rev. D* **65**, 033007 (2002).
[57] J. Pumplin *et al.*, *J. High Energy Phys.* **07**, 012 (2002).
[58] J. M. Campbell and R. K. Ellis, *Phys. Rev. D* **60**, 113006 (1999).
[59] R. Bonciani, S. Catani, M. L. Mangano, and P. Nason, *Nucl. Phys. B* **529**, 424 (1998); M. Cacciari *et al.*, *J. High Energy Phys.* **04**, 068 (2004).
[60] D. Choudhury, S. Majhi, and V. Ravindran, *Nucl. Phys. B* **660**, 343 (2003); W. Shao-Ming *et al.*, *Phys. Rev. D* **74**, 0579002 (2006).
[61] T. Sjöstrand, *Comput. Phys. Commun.* **82**, 74 (1994).
[62] C. Ciobanu *et al.*, *FERMILAB-FN-0773-E* (2008).
[63] J. L. Rosner, *Phys. Rev. D* **54**, 1078 (1996).
[64] K. Cheung and G. Landsberg, *Phys. Rev. D* **62**, 076003 (2000).
[65] V. M. Abazov *et al.* (D0 Collaboration), *Phys. Rev. Lett.* **102**, 051601 (2009); V. M. Abazov *et al.* (D0 Collaboration), *Phys. Rev. Lett.* **95**, 161602 (2005); B. Abbott *et al.* (D0 Collaboration), *Phys. Rev. Lett.* **86**, 1156 (2001).
[66] T. Aaltonen *et al.* (CDF Collaboration), *Phys. Rev. Lett.* **103**, 092002 (2009); V. M. Abazov *et al.* (D0 Collaboration), *Phys. Rev. Lett.* **103**, 092001 (2009); T. Aaltonen *et al.* (CDF Collaboration), *arXiv:0908.3534v1* (2009); T. Aaltonen *et al.* (CDF Collaboration), *Phys. Rev. Lett.* **103**, 101802 (2009).
[67] T. Aaltonen *et al.* (CDF Collaboration), *Phys. Rev. Lett.* **102**, 152001 (2009); T. Aaltonen *et al.* (CDF Collaboration), *Phys. Rev. D* **79**, 072010 (2009); T. Aaltonen *et al.* (CDF Collaboration), *Phys. Rev. Lett.* **99**, 182002 (2007); V. M. Abazov *et al.* (D0 Collaboration), *Phys. Rev. D* **74**, 092005 (2006).